Multilayer Graphene Enables Higher Efficiency in Improving Thermal Conductivities of Graphene/Epoxy Composites – Supporting Information

[1]Xi Shen, [1]Zhenyu Wang, [1]Ying Wu, [1]Xu Liu, [2]Yan-Bing He and [1]Jang-Kyo Kim*

[1]Department of Mechanical and Aerospace Engineering, The Hong Kong University of Science and Technology, Clear Water Bay, Kowloon, Hong Kong

[2]Engineering Laboratory for Functionalized Carbon Materials, Graduate School at Shenzhen, Tsinghua University, Shenzhen 518055, China

*To whom correspondence should be addressed: mejkkim@ust.hk

S1. Calculation of heat flux and temperature

The heat flux J was generated by constantly exchanging the velocity vector of the atom with the highest kinetic energy (i.e., hottest atom) at one end with that of the atom with the lowest kinetic energy (i.e., coldest atom) at the other end:

$$J = \frac{1}{At}\Sigma_{transfer}(\frac{1}{2}m_h v_h{}^2 - \frac{1}{2}m_c v_c{}^2) \tag{1}$$

where A is the cross-sectional area; t is the total time of the exchange process; m and v are the atomic mass and velocity of the atoms, respectively; subscript h and c correspond to the hottest and coldest atoms, respectively. The model along the heat flux direction was divided into several slabs, and the temperature in the kth (k = 1, 2, 3…) slab was calculated as

$$T_k = \frac{1}{3n_k k_B} \sum_{i \in k}^{n_k} m_i v_i{}^2 \tag{2}$$

where n_k is the number of atoms in the kth slab; k_B is the Boltzmann constant; m_i and v_i are the mass and velocity of the ith atom in the kth slab, respectively.

S2. TC of embedded graphene

Similar to the case of suspended graphene,[1] the TC of embedded graphene in epoxy depends on its length at nanometer scale due to the boundary scattering. Therefore, we use a similar scaling method[2,3] to extrapolate the TC of embedded graphene with different n when the lengths of graphene sheets are in micrometer scale. The TC, κ, is proportional to the mean free path for phonon scattering:

$$\frac{1}{\kappa} \propto \frac{1}{l_{ph}} + \frac{1}{l_g} \tag{3}$$

where l_{ph} is the phonon MFP due to phonon-phonon scattering and l_g is the scattering length due to the boundaries, which can be estimated as the length of graphene sheet. According to the above relationship, $1/\kappa$ is plotted as a function of $1/l_g$, as shown in Figure S1. The reciprocals of intercepts from the linear fittings correspond to the TCs of graphene with different n. The TCs of graphene sheets containing 1, 5 and 10 layers are 1206, 1580 and 1670 W/mK, respectively.
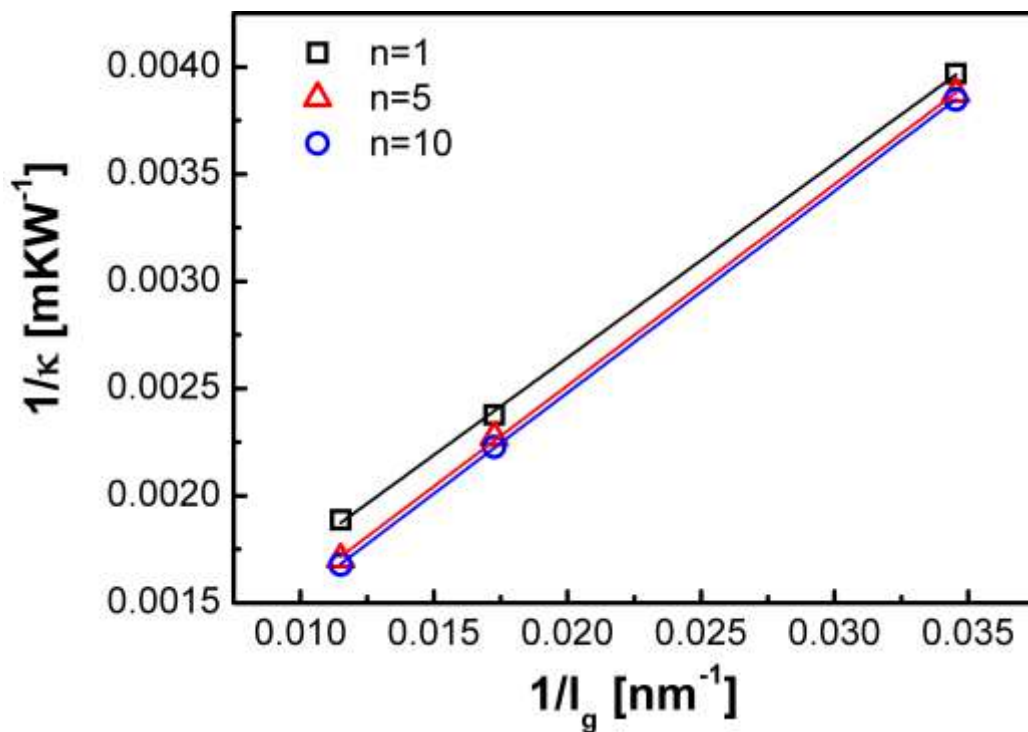
Figure S1. Plot of $1/\kappa$ as a function of $1/l_g$ of graphene sheets with different number of layers.

S3. Sizes and thicknesses of GNPs

The size distributions of the two groups of GNPs measured by the Particle Size Analyzer (COULTER LS 230) are shown in Figure S2a. The mean sizes of GNPs drastically reduced from 34.4 to 1.7 μm when the sonication time increased from 8 to 20 h as GNPs were fragmented into smaller pieces by sonication. Such different sizes of GNPs were further confirmed by the scanning electron microscope (SEM) images (see insets of Figure S2a). The thicknesses of GNPs determined from the atomic force microscopy (AFM) were ~21 and ~15 nm, respectively for GNP-8 and GNP-20, as shown in Figure S2b. Compared to the huge difference in lateral size between the two groups of GNPs, the difference in thickness was almost negligible, indicating that sonication was ineffective in exfoliating GNPs.
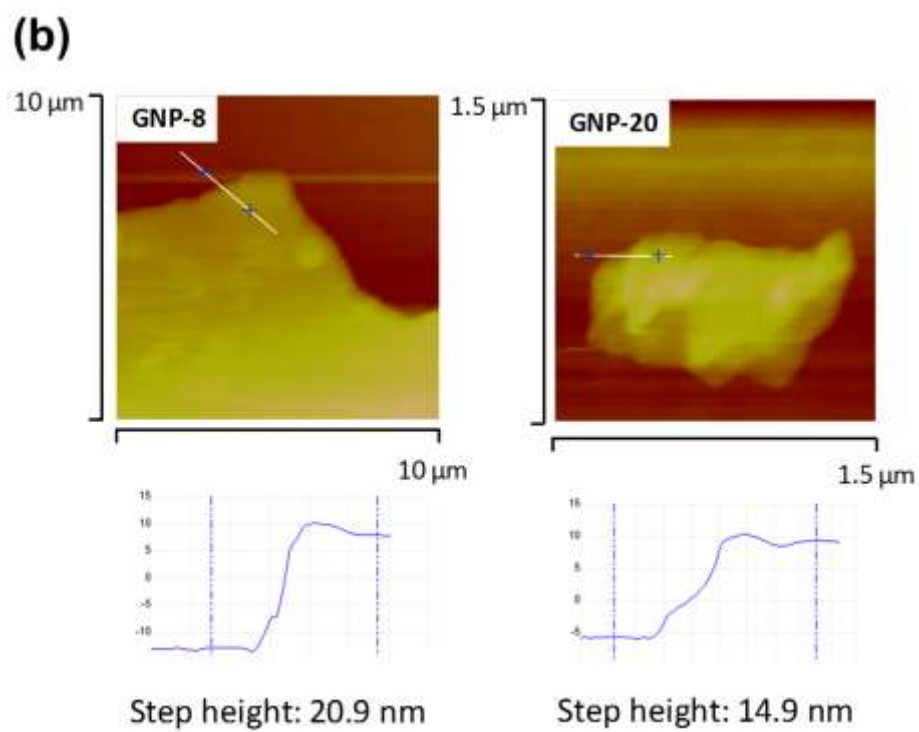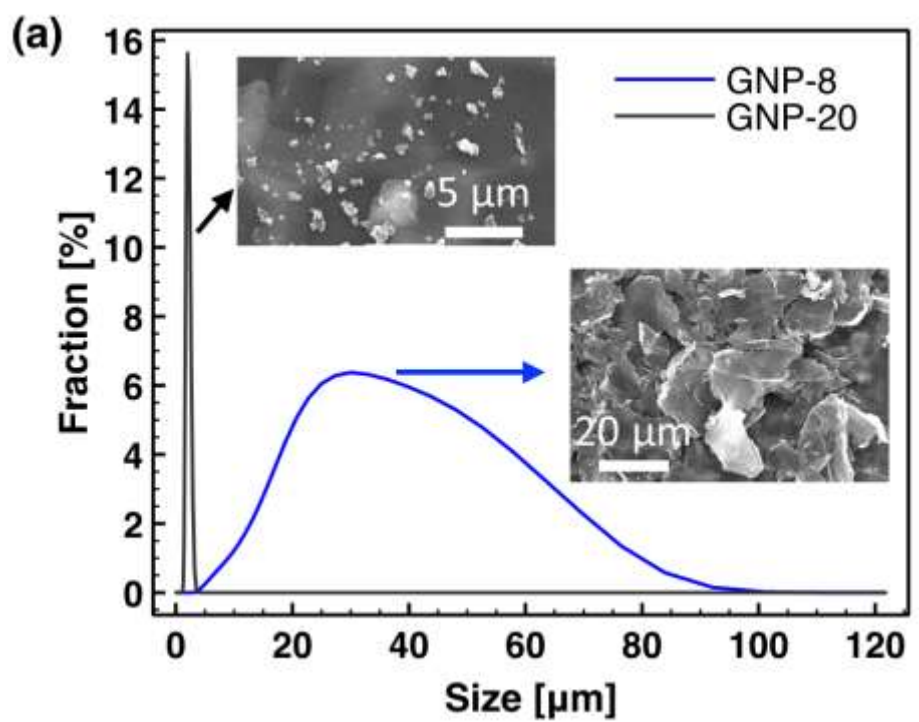
Figure S2. (a) Size distributions of two groups of GNPs with insets showing their SEM images;(b) AFM images and the step profiles of GNPs.

S4. Preparation of GNPs/epoxy composites

The desired amount of GNPs was first weighted according to the filler loading, and then dispersed in acetone at a concentration of 2 mg/mL. The epoxy resin (LY1564, provided by Huntsman Advanced Materials) was added to the GNPs-acetone solution. To avoid further reduction of GNPs size during the process of composites, we used only mechanical stirring and shear mixing to disperse GNPs in epoxy. The mixture containing GNPs, epoxy resin and acetone was mechanically stirred for 30 min, followed by mixing using a high shear mixer at 1000 rpm for 30 min at room temperature. The homogenous mixture was then mechanically stirred on a hot plate at 60 °C until acetone evaporated. The hardener (XB3403, provided by Huntsman Advanced Materials) was then added to the mixture at the ratio of 12:100 of epoxy, followed by degassing in a vacuum oven at 60 °C for 2 h to eliminate entrapped air and residual acetone. The mixture was poured into a silicone mold and cured at 80 °C for 0.5 h and post-cured at 120 °C for 1.5 h. Composite samples containing two groups of GNPs with different sizes were prepared at various filler loadings.
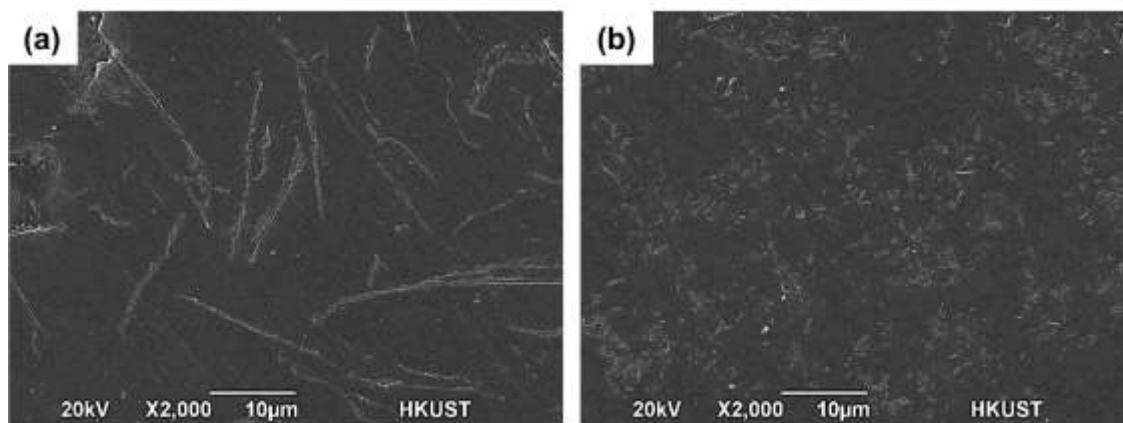
Figure S3. SEM images of GNP/epoxy composites containing 2.8 vol% (equivalent to 5 wt%) of (a) GNP-8 and (b) GNP-20.
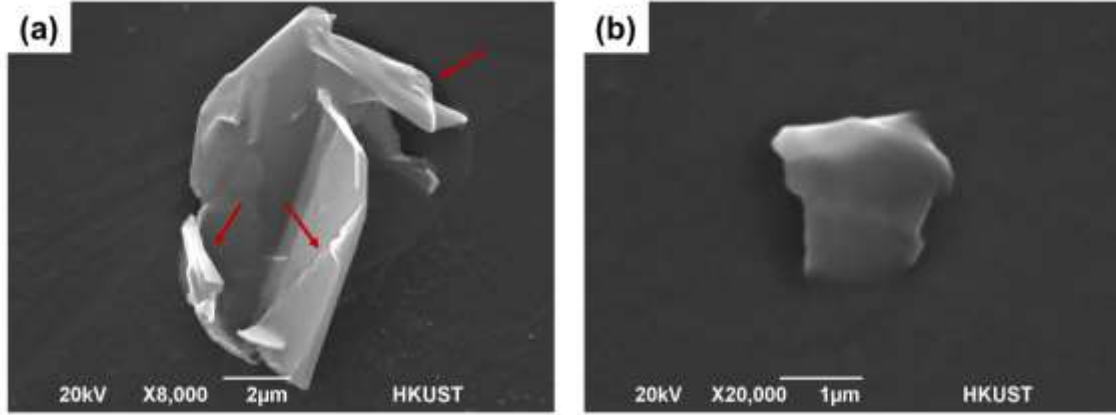
Figure S4. SEM images of (a) GNP-8 and (b) GNP-20. Red arrows indicate folding and wrinkles in GNP-8 due to extremely high aspect ratios.

S5. Apparent TCs and thermal contact resistance

For practical applications of TIMs, the performance of TIMs was characterized by its thermal resistance, $R_{TIM} = H/\kappa + 2R_c$, where H is the bond line thickness (BLT), κ is the intrinsic TC of the TIM and R_c is the thermal contact resistance between the TIM and bonding surfaces. Therefore, R_c also plays a role in determining the performance of TIMs. The apparent TC, $\kappa_A \equiv H/R_{TIM}$, which includes the contribution from the thermal contact resistance, is usually used for comparison of the performance of TIMs.[4] To measure the apparent TCs of composites, we prepared Cu-composites-Cu sandwich samples.[4] A thin Cu foil (~15 μm) was first placed on the bottom of the mold. The mixture of GNPs and epoxy was poured onto the mold. Another thin Cu foil was subsequently placed on top and a glass slide was used to apply even pressure on the top Cu foil. The thickness of the sandwich sample was controlled by the depth of the mold. The total thickness of the sample was ~300 μm, giving a BLT of ~ 270 μm. The sandwich structure was then cured in an oven at 80 °C for 0.5 h and post-cured at 120 °C for 1.5 h. The solid samples were cut into disc shapes of 12.7 mm in diameter for TC measurements.

The apparent TCs of the composites containing 2.8 vol% GNP-8 and GNP-20 were measured using the laser flash technique, and the results are shown in Figure S5. The thermal contact resistance was calculated using the equation,[4] $R_c = \frac{1}{2}(\frac{H}{\kappa} - \frac{H}{\kappa_A})$, and compared with other materials in Table S1.
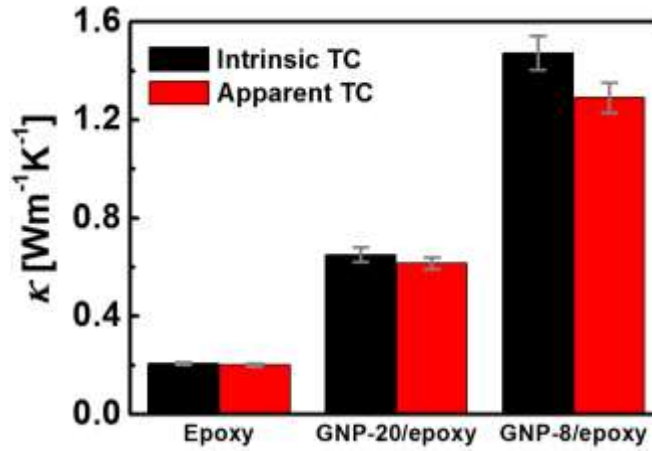
Figure S5. Apparent TCs of epoxy and its composites in comparison with their intrinsic TCs.

Table S1. Comparison of apparent TCs and thermal contact resistance of different types of TIMs.

Type of TIM	Filler content (vol %)	κ_A (W/mK)	$\kappa_A/\kappa_{m,A}$	$R_{contact}$ (mm^{2}K/W)
GNP-20/epoxy (Current work)	2.8	0.62	3.08	11.9
GNP-8/epoxy (Current work)	2.8	1.29	6.42	13.4
FLG/thermal grease[4]	3.4	~1.3	~2	<20
Aligned FLG/epoxy[4]	0.55	~0.32	~3.2	<20
Graphene-MLG/thermal grease[5]	2	~ 14	~2.4	N/A

|					
CNT bucky papers[6]	N/A	~1.59	N/A	40.5
Commercial Al/epoxy[7]	N/A	~0.7	N/A	31
Commercial RTV silicone[7]	N/A	~0.5	N/A	7.9

Notes: FLG: few-layer graphene; MLG: multilayer graphene; RTV: room temperature vulcanization.

S6. Cross-linking process of epoxy

Many methods[8-11] have been proposed to construct cross-linked models of epoxies whose properties are in agreement with experiments. In the present study, a common and reliable method[10] was adopted to create epoxy models with a realistic degree of conversion. The cross-linking process began with identifying the available reaction sites in both DGEBF and TETA molecules, i.e., the end carbon atoms (labeled as R1) in DGEBF molecules and nitrogen atoms (labeled as R2) in TETA molecules (Figure S6). Then an initial cutoff distance for chemical reaction was set at 3 Å. If the distance between any R1 and R2 fell within this cutoff distance, the epoxy ring attached to R1 opened and a new bond was created between R1 and R2. After all available R1 and R2 reacted, the extra hydrogen atoms were removed and partial charges were recalculated. The new structure was subsequently relaxed by energy minimization, followed by NVT dynamics run to eliminate high internal stresses. The above cross-linking process recurred with an increased cutoff distance by 1 Å until the degree of conversion of the system reached 70 %.
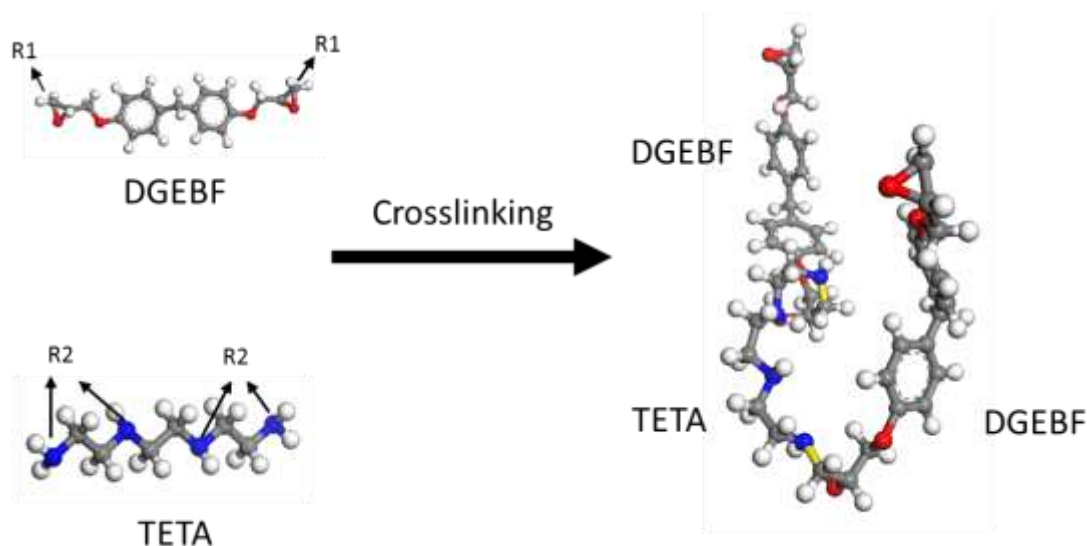
Figure S6. Schematic showing the cross-linking process of epoxy where two DGEBF molecules crosslink with one TETA molecule. The newly formed covalent bonds are highlighted in yellow.

S7. Effect of the shape of GNPs

The shapes of GNPs in real samples are usually irregular. Assuming GNPs with different shapes have the same basal plane surface area to thickness ratio, the change in the shape may cause changes in edge perimeter and edge surface area. To provide a qualitative understanding of such an effect, the ratio of edge surface area to plane surface area, A_{edge}/A_{plane}, is plotted as a function of length to width ratio (a/b), as shown in Figure S7. Here, we assumed that the rectangular-shaped GNPs with different a/b ratios had the same basal plane surface area as the disc-shaped GNP; and $r/t \sim 1000$ for the disc-shaped GNP.

For the disc-shaped GNPs, the area ratio, A_{edge}/A_{plane}, was only 0.1% because of the inherently smallest edge perimeter among all shapes with the same plane surface area. For rectangular-shaped GNPs, although the edge surface area increased with increasing a/b, it was negligible compared to the basal plane surface area. Even when a/b was increased to 1000, the edge surface area was less than 2% of the basal plane surface area.

Assuming the contribution of interfacial heat conduction between GNPs and the epoxy matrix was approximately proportional to the contact surface area, the shape and width to length ratio of GNPs had a negligible influence on the thermal properties of composites judging from the very small edge to plane surface area ratios for all cases considered.
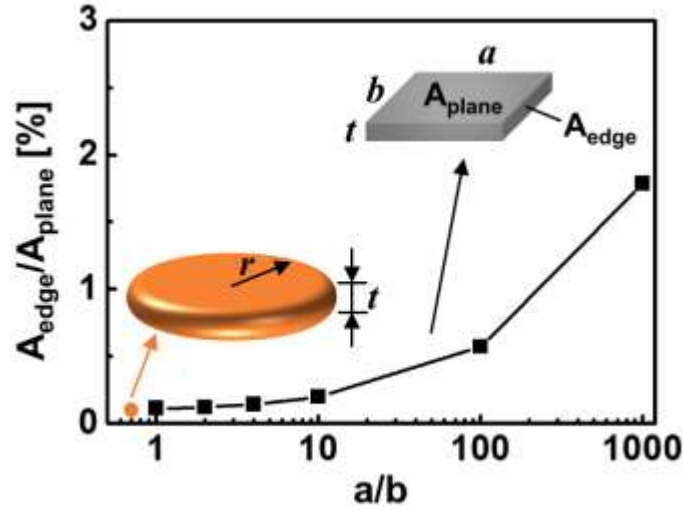
Figure S7. Plot of the area ratio, A_{edge}/A_{plane}, as a function of length to width ratio, a/b. The inset schematics show the dimensions of disc- and rectangular-shaped GNPs. It is assumed the basal plane surface area to thickness ratios of all GNPs of different shapes are identical.

S8. Detailed derivation of the analytical model

The effective medium theory gives the TC of the composite as:[12]

$$\kappa_x = \kappa_m \frac{1+f[\beta_z(1-L_z)(1-\langle\cos^2\theta\rangle)+\beta_x(1-L_x)\langle\cos^2\theta\rangle]}{1-f[\beta_z L_z(1-\langle\cos^2\theta\rangle)+\beta_x L_x\langle\cos^2\theta\rangle]}, \tag{4}$$

$$\kappa_y = \kappa_z = \kappa_m \frac{2+f[\beta_z(1-L_z)(1+\langle\cos^2\theta\rangle)+\beta_x(1-L_x)(1-\langle\cos^2\theta\rangle)]}{2-f[\beta_z L_z(1+\langle\cos^2\theta\rangle)+\beta_x L_x(1-\langle\cos^2\theta\rangle)]}, \tag{5}$$

with

$$\beta_i = \frac{\kappa_i^c - \kappa_m}{\kappa_m + L_i(\kappa_i^c - \kappa_m)}, \text{ for } i = x, y \text{ and } z, \tag{6}$$

10

$$\langle \cos^2 \theta \rangle = \frac{\int \rho(\theta) \cos^2 \theta \sin \theta \, d\theta}{\int \rho(\theta) \sin \theta \, d\theta} \, . \tag{7}$$

In the above equations, κ_x, κ_y, and κ_z are the TC of composites along x-, y- and z- axis, respectively; θ is the angle between global axis x and local axis x'; $\rho(\theta)$ is the distribution function of θ; κ_m is the TC of the matrix; f is the volume fraction of graphene; L_i ($i = x$, y and z) is a geometric factor related to the particle shape, $p = {}^h/_D$, and is given by:

$$L_y = L_z = \frac{p^2}{2(p^2-1)} + \frac{p}{2(1-p^2)^{3/2}} \cos^{-1} p \, , \tag{8}$$

$$L_x = 1 - 2L_y \, . \tag{9}$$

The equivalent TC of composites along the i-axis ($i = x$, y and z), κ_i^c, is given by

$$\kappa_i^c = \frac{\kappa_p}{1+(1+2p)R_I L_i \kappa_p / h}, \tag{10}$$

where R_I is the interface resistance; κ_p is the TC of graphene.

For randomly oriented graphene sheets in the matrix, $\langle \cos^2 \theta \rangle = 1/3$.[8] Therefore, the effective TC of composites, κ_{eff}, is reduced to:

$$\kappa_{eff} = \kappa_x = \kappa_y = \kappa_z = \kappa_m \frac{3+f[2\beta_z(1-L_z)+\beta_x(1-L_x)]}{3-f(2\beta_z L_z + \beta_x L_x)} \, . \tag{11}$$

By replacing the thickness-dependent $\kappa_p(n)$ and $R_I(n)$ into the equations (10), (6), and then (11), the final equation for calculating TC of bulk composites is obtained:

$$\kappa_{eff}(n) = \kappa_m \frac{3+f\left[2\frac{\kappa_z^C(n)-\kappa_m}{\kappa_m+L_z(\kappa_z^C(n)-\kappa_m)}(1-L_z)+\frac{\kappa_x^C(n)-\kappa_m}{\kappa_m+L_x(\kappa_x^C(n)-\kappa_m)}(1-L_x)\right]}{3-f\left(2\frac{\kappa_z^C(n)-\kappa_m}{\kappa_m+L_z(\kappa_z^C(n)-\kappa_m)}L_y+\frac{\kappa_x^C(n)-\kappa_m}{\kappa_m+L_x(\kappa_x^C(n)-\kappa_m)}L_x\right)} \, . \tag{12}$$

References

(1) Shen, X.; Lin, X.; Jia, J.; Wang, Z.; Li, Z.; Kim, J.-K. *Carbon* **2014**, *80*, 235–245.

(2) Bagri, A.; Kim, S.; Ruoff, R. S.; Shenoy, V. B. *Nano Lett.* **2011**, *11* (9), 3917–3921.

(3)   Mu, X.; Wu, X.; Zhang, T.; Go, D. B.; Luo, T. *Sci. Rep.* **2014**, *4* , 3909.

(4)   Renteria, J.; Legedza, S.; Salgado, R.; Balandin, M. P.; Ramirez, S.; Saadah, M.; Kargar, F.; Balandin, A. A. *Mater. Des.* **2015**, 88, 214–221.

(5)   Shahil, K. M. F.; Balandin, A. A. *Nano Lett.* **2012**, *12* (2), 861–867.

(6)   Chen, H.; Chen, M.; Di, J.; Xu, G.; Li, H.; Li, Q. *J. Phys. Chem. C* **2012**, *116* (6), 3903–3909.

(7)   Teertstra, P. In *ASME 2007 InterPACK Conference, Volume 1*; ASME, 2007; pp 381–388.

(8)   Wu, C.; Xu, W. *Polymer* **2006**, *47* (16), 6004–6009.

(9)   Li, C.; Strachan, A. *Polymer* **2010**, *51* (25), 6058–6070.

(10)   Shenogina, N. B.; Tsige, M.; Patnaik, S. S.; Mukhopadhyay, S. M. *Macromolecules* **2012**, *45* (12), 5307–5315.

(11)   Yu, S.; Yang, S.; Cho, M. *Polymer* **2009**, *50* (3), 945–952.

(12)   Nan, C.-W.; Birringer, R.; Clarke, D. R.; Gleiter, H. *J. Appl. Phys.* **1997**, *81* (10), 6692.